ARTICLE

Current Imaging and Electromigration-Induced Splitting of GaN Nanowires As Revealed by Conductive Atomic Force Microscopy

Chun Li,* Yoshio Bando, and Dmitri Golberg

International Center for Materials Nanoarchitectonics (MANA), National Institute for Materials Science (NIMS), Namiki 1-1, Tsukuba, Ibaraki 305-004, Japan

ABSTRACT Current images of electromigration-induced common vapor—liquid—solid-grown GaN nanowires were obtained using a conductive atomic force microscope. Structural characterization indicated that these wurtzite (ZW) [01$\bar{1}$0] nanowires contained longitudinal zinc blende (ZB) defects as stacking faults. The current was attributed to tunneling current through the Schottky barrier between the AFM tip and a nanowire, which was dominated by the local nanowire surface work function. Due to the electromigration induced by large current densities around the defects, the axial splitting process of the nanowires was directly observed under continuous current scanning. The electromigration was likely enhanced by non-uniformly distributed electrostatic pressure around the axial ZW/ZB domain interfaces.

KEYWORDS: gallium nitride · atomic force microscopy · semiconducting nanowire · electromigration · surface potential

The electrical current flow through a solid can produce intense atomic motion (known as electromigration) due to a momentum transfer between flowing electrons and diffusing atoms. This phenomenon can lead to morphological instabilities not only on a metallic surface but also on the semiconductor surfaces.[1] Much research has been focused on the electromigration effects due to their practical importance for the electronic device performance and its stability. Recently, semiconducting nanowires have been given prime attention in light of their usage as low-dimensional platforms for fundamental research and as building blocks for future nanoscale circuits.[2,3] As a structure size in electronics decreases to hundreds/tens of nanometers, local fluctuations, such as interfacial effects, variations in composition, and defects (*i.e.*, dislocations), can dramatically affect a carrier transport. Thus, electromigration becomes the key issue that controls the stability and lifespan of a nanoscale device. The electromigration detection methods may be classified into two categories: (i) indirect methods, for example, the measurements of an electrical resistance that increases due to vacancy formation in a wire; (ii) direct visualizations of the wire shapes by using *in situ* transmission or scanning electron microscopes (TEM or SEM). Due to unique capabilities of simultaneous current and topography measurements under decent spatial resolution,[4−6] conductive atomic force microscopy (C-AFM) can be expected to be an efficient tool to get deep insights into the electromigration effects in nanowires. Such study would provide a better understanding of the nanowire's local transport properties relative to its morphology and further information of crystal structures.

Gallium nitride (GaN), a robust wide band gap (3.39 eV) semiconductor, has extensively been used in blue and UV light-emitting diodes (LEDs). With a high melting point, high carrier mobility, and high electrical breakdown field, it is also a prime candidate for future high-power optoelectronic devices.[7] GaN nanowires (NWs) exhibit low lasing thresholds for the UV nanolasers, and their heterojunctions have been demonstrated to be high-efficient visible LEDs. Although GaN normally prefers to be in a wurtzite (WZ) crystal structure, WZ GaN NWs grown *via* a common vapor−liquid−solid (VLS) process often contain numerous stacking defects composed of metastable zinc blende (ZB) GaN phase regions, and bicrystals made of twinned GaN NWs were also reported.[8,9] These defects may influence the luminescence by introducing additional electronic states[10] and/or may lead to a negative differential resistance due to acceptor-like defect levels.[11] In this work, through current mapping of individual GaN NWs by C-AFM, we show that

*Address correspondence to LI.Chun@nims.go.jp, whulic@gmail.com.

Received for review February 4, 2010 and accepted March 4, 2010.

Published online March 17, 2010.
10.1021/nn100223j

© 2010 American Chemical Society

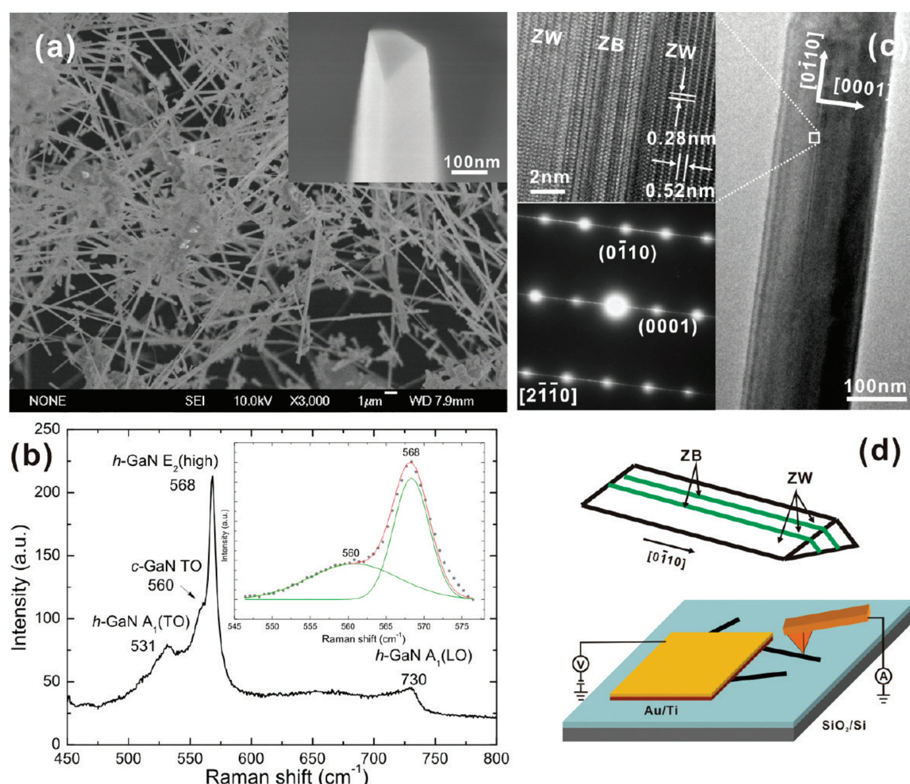

Figure 1. (a) Low- and high-magnification (inset) SEM images of the as-synthesized GaN NWs. (b) Raman spectrum of the GaN NWs excited by an Ar^+ laser with a wavelength of 514.5 nm. The inset shows the results of Gaussian curve fitting for two individual peaks at 560 and 568 cm^{-1}. (c) Typical TEM image of a GaN NW with the corresponding SAED pattern (bottom) and HRTEM images of the inner (top) local regions shown in the inset. (d) Schematic diagram of the geometrical configuration of a GaN NW (top) and an electrical measurement (bottom) by the C-AFM.

these defects can act as the electrical paths with localized high current densities. This drastically enhances the electromigration effects. Subsequently, axial splitting of NWs under continuous current scans has taken place. The possible enhancement of electromigration due to the tip-induced highly non-uniform electrostatic pressure is also discussed.

RESULTS AND DISCUSSION

The GaN NWs were synthesized by metal-catalyzed chemical vapor deposition (CVD) in a tube furnace.[11] Figure 1a shows that the as-synthesized NWs are 100−400 nm in width and several tens of micrometers in length. The typical NW cross sections are triangular or trapezoid in shape (inset of Figure 1a). A Raman spectrum in Figure 1b reveals the first-order phonon frequencies of A_1(TO), E_2(high), and A_1(LO) at 531, 568, and 730 cm^{-1}, respectively, peculiar to a hexagonal GaN (WZ, *h*-GaN).[12] A shoulder at 560 cm^{-1} corresponding to the TO component of the T_2 mode for a cubic GaN phase (ZB, *c*-GaN) is also detected.[13] The detailed crystal structure was further analyzed by TEM shown in Figure 1c. The selected area electron diffraction (SAED) (lower inset of Figure 1c) taken along the [2$\bar{1}\bar{1}$0] zone axis (WZ structure) of a typical NW indicates that the wire grows along the [01$\bar{1}$0] direction. The alternations of WZ and ZB phases along the NW transverse direction result in strip lines and corresponding weak diffraction spots along the [01$\bar{1}$0] direction. This is further confirmed by the HRTEM images of near-perfect WZ lattice intervened with few nanometer-width ZB stacking faults (the top inset of Figure 1c) in line with the published data.[10] The existence of such longitudinal interfacial defects usually leads to the nonsmooth NW lateral surface. The geometrical configuration of these two phases can be illustrated in the inset of Figure 1d. Note that the similar WZ/ZB heterostructures have also been observed in other hexagonal crystals such as ZnS,[14] InAs,[15] and ZnO.[16] The formation of such structures is thought to result from possible doping or strain accumulation and relaxation during the growth, in accord with the defect-mediated VLS model.[8−10]

The samples for C-AFM measurements were fabricated on a SiO_2/Si substrate, as depicted in the schematic diagram of Figure 1d. After patterned deposition of a Ti/Au film by the photolithography, a rapid thermal annealing (RTA) process was performed to form Ohmic contacts between the NWs and the Ti/Au film. The Cr/Au-coated Si cantilever was used as an AFM tip. The observations of the similar NW splitting processes were monitored during independent experiments on more than 10 randomly selected NWs. The typical current value varied from 0.1 to several nanoamperes. The representative topography and the corresponding current

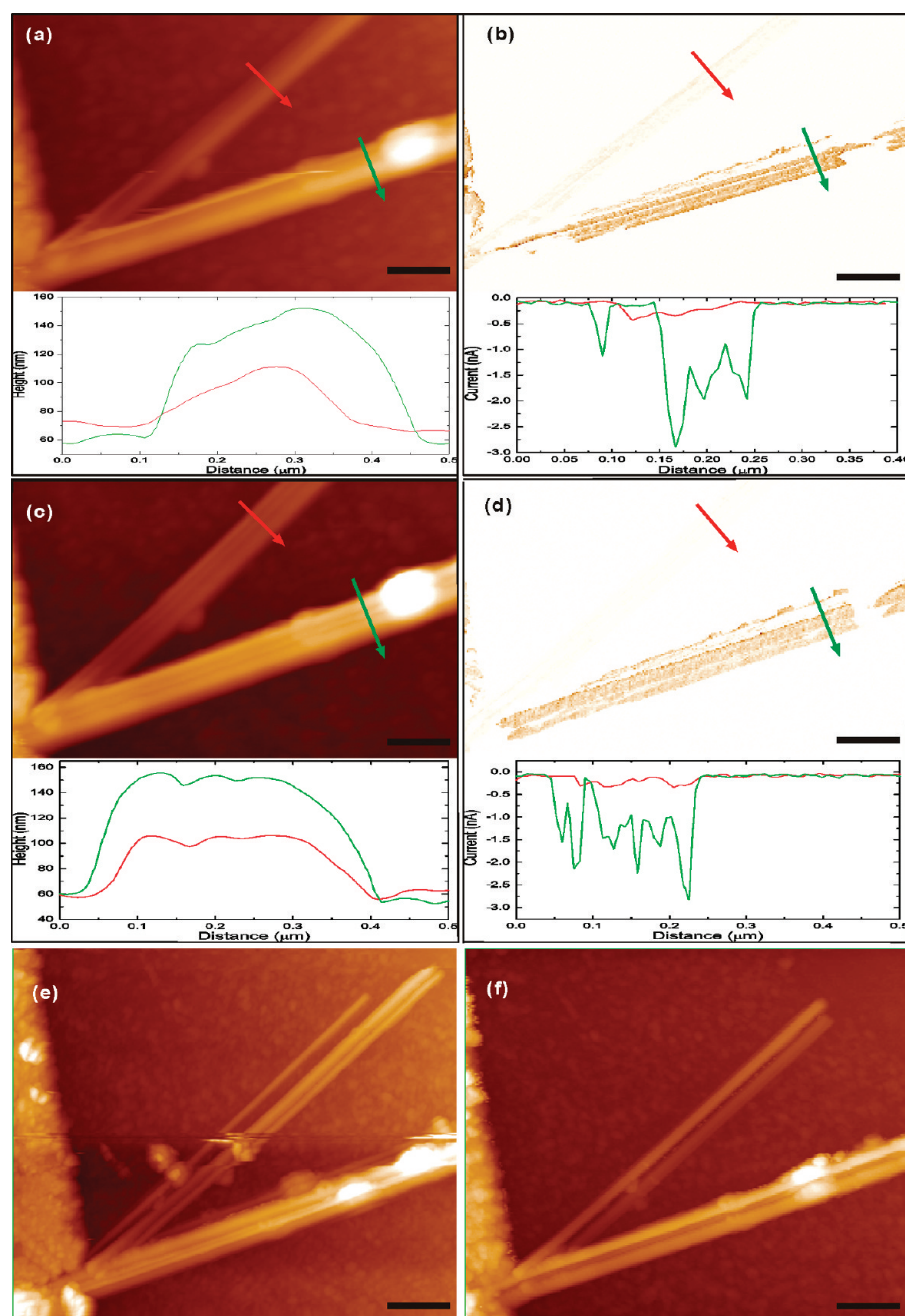

Figure 2. AFM topography images of continuous first (a) and second (c) scans, with the corresponding current images shown in (b) and (d), respectively. The height and current profile curves for each NW are also shown. A bias voltage of −3 V was applied to the sample. (e,f) Tapping-mode AFM images after five consecutive scans and after 10 h of current scanning process, respectively. The scans start from the left-top image corner and end at the right-bottom corner. Scale bars are 500 nm.

images during continuous first and second scans on two NWs with their left-hand-side ends embedded into the electrode are shown in Figures 2a−d. The current images display weak parallel strip patterns, and the current values do not vary along the NW length. Comparing the two scans, we note that the height profile curves from the same positions on each NW clearly change from the original asymmetric triangular shape to a more flat trapezoid shape, while the current variation slightly increases. After five continuous scans, the initial NWs split into several parallel NWs of smaller widths (Figure 2e). Interestingly, we observed that after several hours of a current sensing scanning process, some split NWs disappear and each NW typically shows only two individual parallel branches (Figure 2f).

It is interesting to find out the factors that dominate wire splitting. It was reported that the tip-to-substrate Joule heating current above 1 μA in C-AFM may result in a temperature increase of 100−500 °C based on the heat flow equation,[17,18] $\Delta T = 0.5P_o/\pi KR$ where P_o is the average power dissipated around the contact, K is the thermal conductivity, and R is the

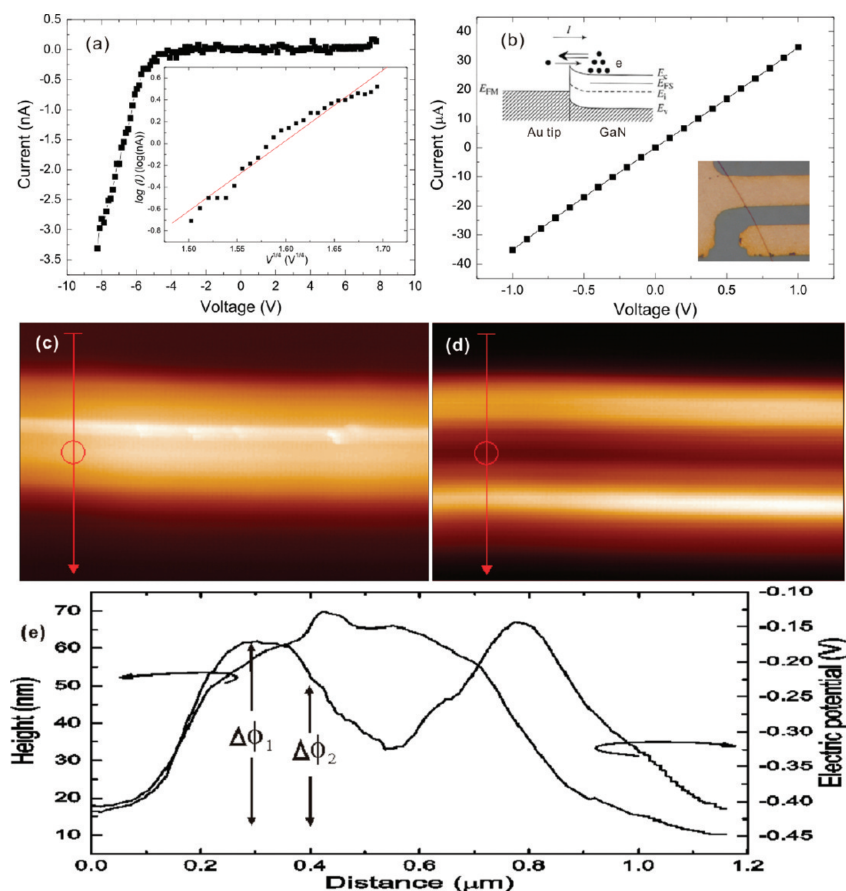

Figure 3. (a) *I*−*V* sweep on the local C-AFM contact point with the inset showing the corresponding logarithmic plot of a backward absolute current value *vs* an applied voltage $V^{1/4}$. Only the data above the turn-on voltage (−4 V) are shown. (b) *I*−*V* curve based on the two-terminal Ti/Au electrode contact measured by a standard probe station. Top inset: band structure diagram shows the Schottky barrier between GaN NW and the Au tip. Bottom inset: optical image of a GaN NW device for probe measurement. (c) Topography and (d) surface potential images of a typical NW on the Au film obtained by SKPM. (e) Height and potential profile curves of the same position are labeled in (c) and (d).

spherical contact radius. Assuming that all of the power *P* dissipated around the contact, and using the values of *R* from a few nanometers (for surface protrusions) to 20 nm (for smooth surface; typical tip radius), and K = 130 W/(m · K) for GaN in our case, we obtained $\Delta T \ll 1$ °C in our case. In fact, a very low current of only a few nanoamperes was indeed involved in the present experiments. Therefore, the possibility of splitting by local thermal shock from Joule heating should be ruled out here. The other possible factor is the high pressure conditions existing between the tip and the NW under small loading forces. However, this was also ruled out based on the observations of no morphology changes under the same scanning conditions without an applied voltage.

In order to investigate the conducting mechanisms, the current−voltage (*I*−*V*) sweeps recorded on the local point of the NW surface by C-AFM and the surface potential measurements by scanning Kelvin probe microscopy (SKPM) were performed in tandem. Figure 3a shows that the *I*−*V* curve clearly exhibits nonlinear and asymmetrical characteristics. Considering the Ohmic contacts between GaN and Ti/Au film after RTA (Figure 3b), and a nearly linear plot of the logarithm of the current value within the $V^{1/4}$ increasing region, it is evident that the transport is dominated by a backward current through the Schottky barrier at the NW/Au tip interface,[19] as shown in the top inset of Figure 3b. It is known that, when AFM scans in a contact mode are taken at ambient conditions, a molecular thin interfacial layer of water and/or contamination of the order of atomic dimensions may appear between the tip and the sample.[20] This interfacial layer may be broken under high electric field and finally gives a Schottky contact between the tip surface and NW. The simplest consideration of the Schottky barrier formation between metals and semiconductors relies on the difference in work functions of the two materials, and the actual barrier height can also be influenced by the existence of surface states which pin the Fermi level at the interface. Figure 3c,d shows the topography and surface potential images of a NW on the Au film, respectively. The height and potential profile curves in Figure 3e indicate that the work function difference of the defective region (longitudinal surface extrusion) between Au ($\Delta\Phi_2$) is smaller than that of near-perfect GaN between

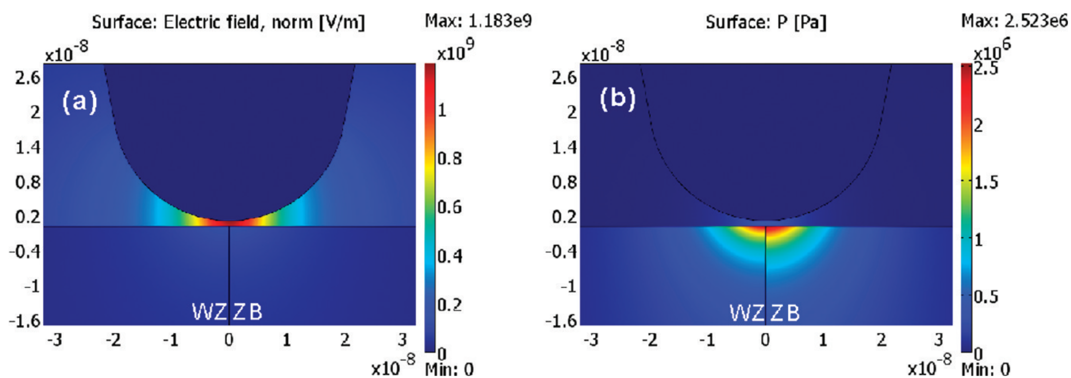

Figure 4. Simulated results of the normalized values for (a) electrical field and (b) electrostatic pressure distributions for a WB/ZB GaN heterojunction at a NW bias voltage of −3 V, tip radius of 20 nm, tip−surface separation of 1 nm, and the dielectric permittivity of air ε_{air} = 1.0548.

Au ($\Delta\Phi_1$) (also see Supporting Information Figure S1). Consequently, the barrier height between the Au-coated tip and the defective region surface is relatively lower. Therefore, the localized surface defects can create the main conductive paths with a larger current, corresponding to current variation and strip patterns in Figure 2b,c. This is consistent with the earlier reports that dislocations with a screw or mixed component are the major current paths in GaN materials grown by different techniques.[21−23] The difference of a current level for each NW might be attributed to the crystal facet dependent work function and the surface state variations.[19] In addition, we also found that after several local *I*−*V* sweeps the NWs had been either broken into several segments due to strong electrical shock or covered with some molten metal from the tip surface attracted by high electrostatic forces, depending on the crystal quality of the NW contact points.

It is known that an electric current flow through a conductor exerts forces on defects in it. When a high electric field or current is applied (for metal interconnects, a current density is above 10^6 A/cm^2),[24] an electric-field-enhanced atomic transport or electromigration occurs.[25] Assuming a few nanometer size for a defective region in the transverse scale and a depth of the surface conducting path, the corresponding current density is estimated to be on the order of 10^3-10^4 A/cm^2. Considering that electromigration prefers to take place at the phase/grain boundaries, defects, and/or dislocations in a conducting solid, the estimated value for the electromigration threshold in the present GaN NWs with distinct defects/stacking faults seems to be reasonable. It should be also pointed out that local high current densities in areas around the dislocations were also suggested to be responsible for the high leakage currents in GaN-based electronic devices.[21]

The physical processes behind the electromigration may be classified into two parts, one referred to as an electron wind force. This results from the momentum transfer during the electron-atom collisions. The direction of this force is the same as that of the electron flow. The other is the direct force of the electrostatic field related to the nominal charge of an atom. For the present n-type semiconducting GaN, in which the carrier existence and shielding of core ions by free electrons should be taken into account, the wind force is much stronger than the reverse electrostatic force. The electron wind force can cause the atoms to transport from the cathode toward the anode, resulting in surface hillock and void formation. The sustained current loading during scans leads to a significant surface morphological change, as verified in Figure 3a,c.

Finally, we discuss a tip-induced high electrical field effect on the electromigration. Considering an idealized approximation for the geometry of a 1 nm dielectric layer of air between a typical conductive tip with a radius of 20 nm and the flat surface of a ZB/ZW GaN heterojunction, we carried out electrostatic simulations using commercial software COMSOL Multiphyicis. The simulated results verify that an applied voltage (−3 V) yields enormously large electrical fields of 10^8-10^9 V/m near the NW surface, as shown in Figure 4a. The corresponding absolute electrostatic pressure was also calculated based on the Clausius−Mossotti equation,[26] $P = \varepsilon_0(\varepsilon - 1)(\varepsilon + 2)/6$, where ε_0 is vacuum permittivity, E is the electric field, and ε is relative permittivity of a dielectric material. The different dielectric constants of ZB and ZW GaN phases ($\varepsilon_{ZB} = 9.7$, $\varepsilon_{WZ} = 8.9$) produce nonuniform and noncontinuous electrostatic pressure distribution surrounding the interface of ZW/ZB domains, as revealed in Figure 4b. The points within the ZB region clearly show larger electrostatic pressure than those in the ZW region for symmetrical areas with respect to the interface. Considering few nanometer protrusions on the actual NW surface and thus shorter (atomic scale) tip−surface distances,[20] such electrostatic pressures and their difference can be increased even more. Although shear modules for a GaN crystal are in the GPa range, the high non-uniform tip-induced electrostatic pressure may be possibly so large that it is able to break chemical bonds at the ZW/ZB domain interface. In turn, the electromigration can be enhanced at the newly generated grain boundaries. The clusters

of a metastable ZB phase can be easily attracted by the electrostatic forces and delivered/rearranged at the local regions with a high contact resistance (see background of Figure 1e,f).[27] Also, these metastable ZB phase-rich clusters or wires may gradually degenerate at ambient conditions. Continuous current scans promote the enlargement of the surface voids at the defective regions which are distributed along the NW axes. Finally, the electrostatic repulsive forces between the adjacent NWs, an applied force on the formed trench, and stress relaxation lead to a complete individual NW splitting.

CONCLUSION

Current images of VLS-grown GaN NWs were recorded by C-AFM. We observed the axial splitting process of GaN NWs under continuous current scanning. This was suggested to be caused by the electromigration. The latter was induced by the local high current densities around the axial defects at the ZB/WZ GaN interfacial regions. We believe that such electromigration might be exacerbated by the tip-induced highly non-uniform distribution of the electrostatic pressure around the interfaces. Our results will be helpful to understand the mechanism of NW morphology change, even degeneration when NWs used as an electron transport channel. Furthermore, due to decent spatial resolution during local electrical property measurements (for example, while using a carbon nanotube with a diameter less than 10 nm as the AFM tip) and high sensitivity of the local defects to tip-induced high electrical fields, the present C-AFM technique should become an efficient tool to characterize/evaluate the electrical stability of the diverse nanoscale materials.

EXPERIMENTAL METHODS

Synthesis and Characterization of GaN Nanowires: The NWs were synthesized by chemical vapor deposition (CVD) in a tube furnace using a powder mixture with equal molar ratios of Ga_2O_3 and graphite as a source material. A sapphire substrate coated with a 5 nm electron beam evaporated Au catalyst film was placed downstream away from the source. The furnace was heated at a rate of 25 °C/min under a constant flow of 100 sccm NH_3 gas and held at 1050 °C for 4 h. After the furnace was naturally cooled to room temperature, a green-gray powder-like product was found on the substrate. The nanowires were characterized by a room temperature Raman spectrometer with an Ar^+ laser excitation wavelength of 514.5 nm, a scanning electron microscope (SEM; JEOL, JSM-6700F), and a high-resolution field-emission transmission electron microscope (TEM; JEOL, JEM-3000F).

Sample Preparation and C-AFM Measurements: The NWs were ultrasonically dispersed in isopropyl alcohol (IPA) and deposited on a Si wafer with a 200 nm thick layer of thermally grown SiO_2. Patterned 10 nm/100 nm Ti/Au square contacts were fabricated by photolithography followed by rapid thermal annealing (RTA) in N_2 at 500 °C for 30 s. No structural and/or surface morphology changes were noted by TEM and AFM on tens of individual NWs dispersed on the DuraSiN TEM grids before and after RTA. The AFM observations and electrical measurements were carried out in a JEOL JSPM-5200 scanning probe microscope at room temperature in air. Si cantilevers coated with Cr/Au were used for electrical conductive measurements, and the tip was grounded. After finding the exact position of the NWs partially embedded in a Ti/Au electrode using a tapping mode, the stage was driven to the desired position using the standard JEOL software. The contact mode with a contact force of ~30 nN, a sample bias of −2 to −4 V, and a scan speed of 780 nm/s was utilized to record the surface topography and current image simultaneously. For the surface potential measurements, the NW IPA solution was dispersed on a Au-coated Si substrate, and the surface potential images were recorded by the frequency-modulated scanning Kelvin probe microscopy (SKPM) in a noncontact mode at vacuum pressure of 1.0×10^{-4} Pa.

Acknowledgment. This work was supported by the International Center for Materials Nanoarchitectonics (MANA), National Institute for Materials Science (NIMS), Tsukuba, Japan, and the Nanotechnology Network Project of the Ministry of Education, Culture, Sports, Science and Technology (MEXT), Japan. We would like to acknowledge valuable discussions with Drs. M.S. Wang and Y.Z. Yao, and continuous technical support of Drs. A. Nukui, I. Yamada, T. Fujita, and N. Fukata.

Supporting Information Available: Results of scanning Kelvin probe microscopy (SKPM) analysis of a typical GaN NW on the Au surface. This material is available free of charge *via* the Internet at http://pubs.acs.org.

REFERENCES AND NOTES

1. Kandel, D.; Kaxiras, E. Microscopic Theory of Electromigration on Semiconductor Surfaces. *Phys. Rev. Lett.* **1996**, *76*, 1114–1117.
2. Law, M.; Goldberger, J.; Yang, P. Semiconductor Nanowires and Nanotubes. *Annu. Rev. Mater. Res.* **2004**, *34*, 83–122.
3. Hu, J. Q.; Bando, Y.; Golberg, D. Novel Semiconductor Nanowire Heterostructures: Synthesis, Analysis, Properties and Applications. *J. Mater. Chem.* **2009**, *19*, 330–343.
4. Dai, H.; E; Wong, W.; Lieber, C. M. Probing Electrical Transport in Nanomaterials: Conductivity of Individual Carbon Nanotubes. *Science* **1996**, *272*, 523–526.
5. Dorozhkin, P. S.; Tovstonog, S. V.; Golberg, D.; Zhan, J.; Ishikawa, Y.; Shiozawa, M.; Nakanishi, H.; Nakata, K.; Bando, Y. A Liquid-Ga-Filled Carbon Nanotube: A Miniaturized Temperature Sensor and Electrical Switch. *Small* **2005**, *1*, 1088–1093.
6. Pingree, L. S.; Reid, O. G.; Ginger, D. S. Electrical Scanning Probe Microscopy on Active Organic Electronic Devices. *Adv. Mater.* **2008**, *21*, 19–28.
7. Pearton, S. J.; Ren, F. GaN Electronics. *Adv. Mater.* **2000**, *12*, 1571–1580.
8. Tham, D.; Nam, C. Y.; Fischer, J. E. Defects in GaN Nanowires. *Adv. Funct. Mater.* **2006**, *16*, 1197–1202.
9. Liu, B.; Bando, Y.; Tang, C.; Xu, F.; Hu, J.; Golberg, D. Needle-like Bicrystalline GaN Nanowires with Excellent Field Emission Properties. *J. Phys. Chem. B* **2005**, *109*, 17082–17085.
10. Xu, H. Y.; Liu, Z.; Liang, Y.; Rao, Y. Y.; Zhang, X. T.; Hark, S. K. Structure and Photoluminescence of Wurtzite/Zinc-Blende Heterostructure GaN Nanorods. *Appl. Phys. Lett.* **2009**, *95*, 13310-8–13310-10.
11. Chu, W. H.; Chiang, H. W.; Liu, C. P.; Lai, Y. F.; Hsu, K. Y.; Chung, H. C. Defect-Induced Negative Differential Resistance of GaN Nanowires Measured by Conductive Atomic Force Microscopy. *Appl. Phys. Lett.* **2009**, *194*, 182101–182103.
12. Bae, S. Y.; Seo, H. W.; Park, J.; Yang, H.; Kim, H.; Kim, S. Triangular Gallium Nitride Nanorods. *Appl. Phys. Lett.* **2003**, *82*, 4564–4566.
13. Tabata, A.; Lima, A. P.; Leite, J. R.; Lemos, V.; Schikora, D.; Schottker, B.; Kohler, U.; As, D. J.; Lischka, K. Micro-Raman Analysis of Cubic GaN Layers Grown by MBE on (001) GaAs Substrate. *Semicond. Sci. Technol.* **1999**, *14*, 318M–322.

ARTICLE

14. Jie, J. S.; Zhang, W. J.; Jiang, Y.; Meng, X. M.; Zapien, J. A.; Shao, M. W.; Lee, S. T. Heterocrystal and Bicrystal Structures of ZnS Nanowires Synthesized by Plasma Enhanced Chemical Vapour Deposition. *Nanotechnology* **2006**, *17*, 2913–2917.
15. Caroff, P.; Dick, K. A.; Johansson, J.; Messing, M. E.; Deppert, K.; Samuelson, L. Controlled Polytypic and Twin-Plane Superlattices in III−V nanowires. *Nat. Nanotechnol.* **2009**, *4*, 50–55.
16. Lazzarini, L.; Salviati, G.; Fabbri, F.; Zha, M.; Calestani, D.; Zappettini, A.; Sekiguchi, T.; Dierre, B. Unpredicted Nucleation of Extended Zinc Blende Phases in Wurtzite ZnO Nanotetrapod Arms. *ACS Nano* **2009**, *3*, 3158–3164.
17. Richter, S.; Cahen, D.; Cohen, S. R.; Gartsman, K.; Lyakhovitskaya, V.; Manassen, Y. Bulk Changes in Semiconductors Using Scanning Probe Microscopy: nm-Size Fabricated Structures. *Appl. Phys. Lett.* **1998**, *73*, 1868–1871.
18. Schneegans, O.; Moradpour, A.; Wang, K.; Leblanc, A.; Molinié, P. Conducting-Probe AFM Nanoscale Joule Heating Yields Charge-Density-Wave Transition Detection. *J. Phys. Chem. B* **2006**, *110*, 9991–9994.
19. Cheng, G.; Wang, S.; Cheng, K.; Jiang, X.; Wang, L.; Li, L.; Du, Z.; Zou, G. The Current Image of a Single CuO Nanowire Studies by Conductive Atomic Force Microscopy. *Appl. Phys. Lett.* **2008**, *92*, 223116–223118.
20. Pablo, P. J.; Martínez, M. T.; Colchero, J.; Gómez, J.; Maser, W. K.; Benito, A. M.; Muñoz, E.; Baró, A. M. Mechanical and Electrical Properties of Nanosized Contacts on Single-Walled Carbon Nanotubes. *Adv. Mater.* **2000**, *12*, 573–576.
21. Simpkins, B.; Yu, S. E. T.; Waltereit, P.; Speck, J. S. Correlated Scanning Kelvin Probe and Conductive Atomic Force Microscopy Studies of Dislocations in Gallium Nitride. *J. Appl. Phys.* **2003**, *94*, 1448–1453.
22. Brazel, E. G.; Chin, M. A.; Narayanamurti, V. Direct Observation of Localized High Current Densities in GaN Films. *Appl. Phys. Lett.* **1999**, *74*, 2367–2369.
23. Pomarico, A. A.; Huang, D.; Dickinson, J.; Baski, A. A.; Cingolani, R.; Morkoc, H. Current Mapping of GaN Films by Conductive Atomic Force Microscopy. *Appl. Phys. Lett.* **2003**, *82*, 1890–1892.
24. Huang, Q.; Lilley, C. M.; Divan, R. An *In Situ* Investigation of Electromigration in Cu Nanowires. *Nanotechnology* **2009**, *20*, 075706–075711.
25. Black, J. R. Electromigration: A Brief Survey and Some Recent Results. *IEEE Trans. Electron Devices* **1969**, *ED-16*, 338–343.
26. Lyuksyutov, S. F.; Vaia, R. A.; Paramonov, P. B.; Juhl, S.; Waterhouse, L.; Ralich, R. M.; Sigalov, G.; Sancaktar, E. Electrostatic Nanolithography in Polymers Using Atomic Force Microscopy. *Nat. Mater.* **2003**, *2*, 468–472.
27. Avouris, P.; Martel, R.; Hertel, T.; Sandstorm, R. AFM-Tip-Induced and Current-Induced Local Oxidation of Silicon and Metals. *Appl. Phys. A: Mater. Sci. Process.* **1998**, *66*, S659–S667.